Kinetics of Polymer Crystallization with Aggregating Small Crystallites

Takashi Konishi,[1,*] Daisuke Okamoto,[1] Daisuke Tadokoro,[1] Yoshitaka Kawahara,[1] Koji Fukao,[2] and Yoshihisa Miyamoto[1]

[1]*Graduate School of Human and Environmental Studies, Kyoto University, Kyoto 606-8501, Japan*
[2]*Department of Physics, Ritsumeikan University, Noji-Higashi 1-1-1, Kusatsu 525-8577, Japan*

(Received 30 September 2021; accepted 18 February 2022; published 11 March 2022; corrected 31 March 2022)

The isothermal crystallization near the glass transition temperature from the melt state of poly (trimethylene terephthalate) has been studied by wide-angle x-ray diffraction (WAXD), small-angle x-ray scattering (SAXS), and optical microscopy. The SAXS and WAXD results show the crystallization mechanism in which the crystalline nodules cover the entire sample with the formation of aggregation regions. The analysis of the SAXS results using Kolmogorov-Johnson-Mehl-Avrami theory indicates that the formation kinetics of the aggregation regions is of three-dimensional homogeneous nucleation type. The analysis of the SAXS profiles using Sekimoto's theory provides the growth velocity and the nucleation rate of the aggregation region. The temperature dependence of the growth velocity of the aggregation region is a natural extrapolation of that of spherulite to the high supercooling region. The temperature dependence of the nucleation rate of the aggregation region is also represented by the parameters of the spherulitic growth rate. The result of the growth velocities of the aggregation region and the spherulite suggests the existence of precursors at the front of the crystal growth.

DOI: 10.1103/PhysRevLett.128.107801

Traditionally, the classical crystallization theory has explained crystal nucleation and growth mechanism; however, recently two-step features of crystallization with the formation of precursor regions has been discussed in experimental [1–6], simulation [7–9], and theoretical studies [10,11].

Semicrystalline polymers do not perfectly crystallize but form a hierarchical structure unlike low molecular materials due to its morphological characteristics. The polymer crystallization model proposed by Lauritzen and Hoffmann as the secondary nucleation and growth process [12] has been traditionally used for investigation of polymer crystallization. The initial stage of the polymer crystallization has been investigated by many researchers [13–34], and the existence of precursors has been pointed out in the early stage of polymer crystallization [13,20,24–27,31–33].

Recently, a large intensity of small angle x-ray scattering in the low wave number region has been observed during the induction period of crystallization near the glass transition temperature T_g for poly(trimethylene terephthalate) (PTT) from the glassy state [35,36]. Electron micrographs of PTT crystallized at 55°C from the glassy state show the crystalline nodular morphology in the nanometer scale separated by an amorphous region [35]. In a previous study [37], we have also investigated the crystallization from both the melt and glass states of PTT, and have revealed the crystallization mechanism in which the crystalline nodules cover the entire sample with the aggregation regions. The purpose of this Letter is to elucidate the kinetics of the polymer crystallization with aggregating the crystalline nodules. In order to achieve this purpose, we have investigated the crystallization processes from the melt state using x-ray techniques and optical microscopy.

The polymer sample used in this study is PTT. The melting and the glass transition temperatures are determined as 233 and 45°C, respectively, by differential scanning calorimetry (DSC). The PTT films of about 150 μm are isothermally crystallized at crystallization temperatures T_c, between 50 and 70°C, from the melt state.

The isothermal crystallization processes are investigated by simultaneous small-angle x-ray scattering (SAXS) and wide-angle x-ray diffraction (WAXD). The camera lengths of WAXD and SAXS are 100 and 4000 mm, respectively. The wavelength λ for WAXD and SAXS is 1.3 Å. The measurements are performed using the beam line BL-40B2 at SPring-8, Nishiharima, Japan. The x-ray camera for SAXS is Pilatus3S 2M (Dectris) that has a larger light-receiving area than the one in the previous study [37], and can cover a wide range of the scattering vector, $q = 4\pi \sin\theta/\lambda$, from 0.002 to 0.16 Å^{-1} in one exposure, where 2θ is the scattering angle. The camera for WAXD is a flat panel detector (Hamamatsu Photonics), and covers from $q = 0.5$ to 3.0 Å^{-1}. The isothermal crystallization process at the crystallization temperature T_c between 90 and 160°C after melting at 280°C for 2 min is observed by a polarized or an optical microscope (Nikon ECLIPSE ME600) in order to measure the growth rate of the crystalline spherulites. The temperature of the samples is

controlled using a Linkam LK300 which gives the cooling rate 300 K/s.

In a previous study, it has been clarified that the crystalline nodules aggregate and that the aggregation regions cover the entire sample of PTT crystallized near T_g. In this Letter, the kinetics of the nodular aggregation region for PTT will be considered using the simple theory proposed by Kolmogorov, Johnson, Mehl, and Avrami (KJMA) theory [38–42]. The KJMA theory predicts the kinetics of nucleation and growth transformations from the metastable phase into the stable phase for nonconserved system as

$$X(t) = 1 - \exp(-Kt^{n_a}), \tag{1}$$

where $X(t)$ is the volume fraction of the stable domains, K is a constant, and n_a is an Avrami exponent.

For the SAXS measurements, the intensity when the crystallization time t_c is zero, $I(q, t_c = 0)$, is subtracted from $I(q, t_c)$, $I_{\rm sub}(q) = I(q, t_c) - I(q, t_c = 0)$. The WAXD profiles in Fig. S1(a) [43] show that PTT quenched to 60 °C at $t_c = 0$ is amorphous. Figures 1(a) and 1(b) show the t_c-dependent SAXS profiles $I_{\rm sub}(q)$ for PTT isothermally crystallized at 60°C from the melt state until and after 260 s, respectively. Since $I_{\rm sub}(q)$ shows different behaviors in the low- and high-q regions, $I_{\rm sub}(q)$ can be given by $I_{\rm sub}(q) = I_L(q) + I_H(q)$, where $I_L(q)$ and $I_H(q)$ represent $I_{\rm sub}(q)$ at $q < 0.02$ Å^{-1} and $q > 0.02$ Å^{-1}, respectively. The intensity $I_L(q)$ decreases with q, and increases with t_c until 260 s and then decreases after 260 s. On the other hand, $I_H(q)$ has a peak against q, and monotonically increases with t_c. The features shown in the SAXS intensity correspond well to those reported by Chuang and coworkers [35] and a previous our study [37].

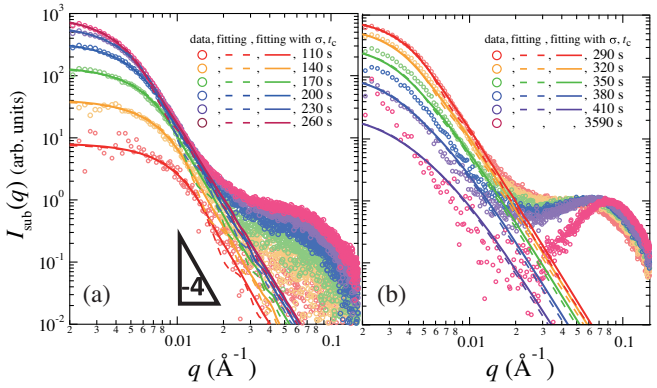

FIG. 1. SAXS profiles $I_{\rm sub}(q)$ as a function of t_c for PTT crystallized at 60 °C from the melt state (a) until and (b) after 260 s. Both the broken and solid curves in (a) and (b) are the theoretical curves obtained using $\tilde{S}_{hng}(q)$ and $\tilde{S}'_{hng}(q)$, respectively, with $v_0 = 2.3$ Å/s and $I_n = 1.26 \times 10^{-11}$ Å^{-3} s^{-1}. The solid curves are calculated using v_0 with a coefficient of variation $\sigma/\bar{v}_0$ of 20%. The right triangle in (a) indicates a slope of −4.

The three-dimensional isotropic SAXS intensity, $I_{\rm tot}(q)$, for the crystallization mechanism with aggregating the nodules has been previously proposed as [37]

$$I_{\rm tot}(q) = I_0(\Delta\rho_{ac})^2\{\chi(1-\chi)\psi^2 S_\eta(q) + \chi\psi(1-\psi)S_\gamma(q)\}, \tag{2}$$

where $S_\eta(q)$, $S_\gamma(q)$ are the normalized structure factors for the aggregation regions in the entire sample and for the nodules in each aggregation region, respectively. χ and ψ are the volume fractions of the aggregation regions and the nodules in each aggregation region, respectively, I_0 is a constant, and $\Delta\rho_{ac}$ is the density difference between the crystal and the amorphous. The volume fraction of the nodules in the entire sample corresponds to the crystallinity $\phi_c = \chi\psi$. $\psi(1-\psi)S_\gamma(q)$ in Eq. (2) can be generally expressed as $\psi V_n|\Phi(q)|^2\mathcal{F}(q)$, where V_n is the volume of the nodule, $|\Phi(q)|^2$ is the normalized form factor for the nodule, and $\mathcal{F}(q)$ is the structure factor for internodules. It has been reported that the distribution of the crystalline nodules is discrete and random since $\mathcal{F}(q)$ can be described as the Percus-Yevick approximation [45] of the hard spheres model [35].

Equation (2) represents the intensity $I_{\rm sub}(q)$ obtained from the SAXS results. The first and second terms in the right-hand side in Eq. (2) should be regarded as $I_L(q)$ and $I_H(q)$, respectively. Assuming constant ψ, the values of χ, χ^Q, ψ, ψ^Q, and ϕ_c, ϕ_c^Q, can be calculated from the invariants of $I_L(q)$ and $I_H(q)$ [37]. The detailed procedure for obtaining χ^Q, ψ^Q, and ϕ_c^Q is described in Sec. 2 in Supplemental Material [43]. The calculation result shows $\psi^Q = 0.246$ and the t_c dependences of χ^Q and ϕ_c^Q $(=\psi^Q\chi^Q)$ depicted in Fig. 2(a). The crystallinity calculated from the WAXD result, ϕ_c^W, in Fig. S1 [43] is depicted in Fig. 2(a). ϕ_c^Q agrees with ϕ_c^W until 400 s in Fig. 2(a). The quantitative agreement indicates that the approximation of constant ψ is valid during the formation of the nodular aggregates. However ϕ_c^W keeps on increasing after 400 s

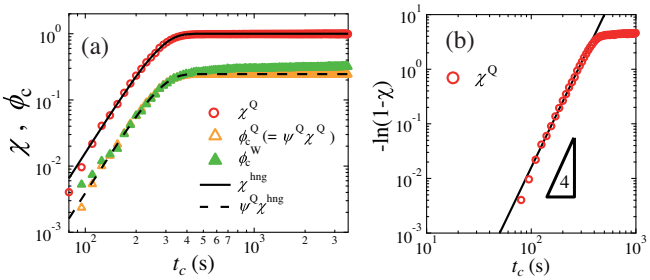

FIG. 2. (a) t_c-dependent χ and ϕ_c obtained from SAXS and WAXD results, and (b) double logarithmic plots of $-\ln(1-\chi)$ against t_c. In (a) solid and broken curves are calculated χ and $\psi\chi$, respectively, using Eq. (1) with $I_n v_0^3 = 1.53 \times 10^{-10}$ s^{-4} and $\psi^Q = 0.246$. The triangle in (b) indicates a slope of 4.

[Figs. 2(a) and S1(c) [43]]. The increase in ϕ_c^W comes from the increase in t_c-dependent ψ due to the thickening of the crystalline nodules or the nucleation of the nodules in the narrow space between the previously formed nodules.

The t_c dependence of χ is analyzed by KJMA theory, regarding X in Eq. (1) as χ. Figure 2(b) shows the double logarithmic plot of $-\ln(1-\chi)$ against t_c. The result shows that $n_a = 4$, that is, the nodular aggregates forms by three-dimensional homogeneous nucleation and growth (3D-homoN&G). Then K becomes $(\pi/3)I_n v_0^3$ where I_n and v_0 are the nucleation rate and the isotropic growth velocity of the aggregation regions, respectively. The value of $I_n v_0^3$ can be estimated as $I_n v_0^3 = 1.53 \times 10^{-10}$ s^{-4}. Figure 2(a) shows that t_c-dependent χ, χ^{hng}, using Eq. (1) with $I_n v_0^3 = 1.53 \times 10^{-10}$ s^{-4} agrees with χ^Q and that $\psi^Q \chi^{hng}$ also agrees with ϕ_c^Q and ϕ_c^W. The quantitative agreement strongly indicates that the formation kinetics of the nodular aggregates is 3D-homoN&G.

Sekimoto has theoretically derived the time dependent structure factor $S_{hng}(q,t)$ of the domains for homogeneous nucleation and growth [46]. The three dimensional isotropic $S_{hng}(q,t)$ can be written as

$$S_{hng}(q,t) = (2\pi)^3 \left[1 - \exp\left(-\frac{\pi}{3} I_n v_0^3 t^3\right)\right]^2 \delta(q) + \tilde{S}_{hng}(q,t), \tag{3}$$

where

$$\tilde{S}_{hng}(q,t) = 4\pi \exp\left(-\frac{2\pi}{3} I_n v_0^3 t^4\right)(2v_0 t)^3 \times \int_0^1 dy y^2 \frac{\sin(2v_0 tyq)}{2v_0 tyq} \{\exp[I_n v_0^3 t^4 \Psi_3(y)] - 1\} \tag{4}$$

and $\Psi_3(y) = \frac{\pi}{3}(1-y)^3(1+y)$. When Eq. (3) is applied to the nodular aggregation system, the first term of $S_{hng}(q,t)$ becomes $(2\pi)^3 \chi^2 \delta(q)$, and $\tilde{S}_{hng}(q,t)$ corresponds to $\chi(1-\chi)S_\eta(q,t)$ in Eq. (2). Thus, when ψ is constant, the $I_L(q,t_c)$ behavior obeys Eq. (4). $I_L(q,t_c)$ is analyzed using Eq. (4) with $I_n v_0^3 = 1.53 \times 10^{-10}$ s^{-4}. Figure 1 shows that the SAXS intensity using Eq. (4) with $v_0 = 2.3$ Å/s and $I_n = 1.26 \times 10^{-11}$ Å^{-3} s^{-1} (the dashed curves) represents $I_L(q,t_c)$ well.

However, comparing $I_L(q)$ and $\tilde{S}_{hng}(q)$ in Fig. 1 in more detail, $\tilde{S}_{hng}(q)$ has oscillation patterns, while $I_L(q)$ has a slope of -4. The oscillation in $\tilde{S}_{hng}(q)$ comes from the form factor in which the maximum size of the ideal spherical domain is definite. Therefore, it is considered that the growth rate v_0 for the nodular aggregation region has the Gaussian distribution, the average $\bar{v}_0$ and the standard deviation σ. The derivation of the structure factor considering the Gaussian distribution of v_0, $\tilde{S}'_{hng}(q)$ [Eq. (S4)], is described in Sec. 3 in the Supplemental Material [43] in detail. Solid curves in Fig. 1 show the calculation curves using $\tilde{S}'_{hng}(q)$ with $\bar{v}_0 = 2.3$ Å/s, $I_n = 1.26 \times 10^{-11}$ Å^{-3} s^{-1}, and a coefficient of variation, $\sigma/\bar{v}_0 = 0.2$. The oscillation patterns in the calculation curves using $\tilde{S}_{hng}(q)$ disappear, and thus $\tilde{S}'_{hng}(q)$ reproduces $I_{\rm sub}(q)$ better than $\tilde{S}_{hng}(q)$. The agreement between $\tilde{S}'_{hng}(q)$ and $I_L(q)$ suggests that the formation kinetics of the nodular aggregates is 3D-homoN&G. The values of v_0 and I_n give the characteristic length $\xi_0 = (v_0/I_n)^{1/4}$ and the characteristic time $\tau_0 = \xi_0/v_0$ in the system. ξ_0 and τ_0 are the typical length and time for the aggregation regions to contact each other, respectively. ξ_0 and τ_0 for $T_c = 60$°C are estimated as 654 Å and 284 s, respectively. t_c at which $I_{\rm sub}(q)$ becomes maximum, t_h, shows $\chi = 0.5$, and equals to $(3 \ln 2/\pi)^{1/4}\tau_0$. t_h for $T_c = 60$°C is estimated as 256 s.

To further investigate the T_c dependences of v_0 and I_n, x-ray measurements of melt-crystallized PTT for different T_c have been performed. Figures S3(a)–S3(d) and S4 show that $I_{\rm sub}(q)$ for different T_c also has $I_L(q)$ and $I_H(q)$ and that these intensities behave similarly to those for $T_c = 60$°C [43]. χ^Q are obtained from $I_L(q)$ by the same procedure for $T_c = 60$°C. The double logarithmic plots of $-\ln(1-\chi)$ against t_c for all T_c in Fig. S5 show that $n_a = 4$ [43]. The result indicates that the kinetics of the nodular aggregation regions for all T_c are 3D-homoN&G. The fittings to $I_L(q)$ for all T_c have been, furthermore, performed using Eq. (S4) with the $I_n v_0^3$ values obtained from Fig. S4 and $\sigma/\bar{v}_0 = 0.2$ [43]. The fitting curves in Figs. S3 and S4 also reproduce $I_L(q)$ well for all T_c and give the values of v_0 and I_n for each T_c [43].

Figure 3(a) shows the T_c dependences of v_0 and I_n. v_0 increases with increasing T_c, while I_n shows the bell shape with the maximal at $T_c = 60$°C. The slowdowns near T_g for both v_0 and I_n indicate that the formation of the aggregates is dominated by the translational diffusion in the media. The slowdown above 60°C for I_n is predicted to come from a sharp increase in the activation energy required for the critical nucleation of the nodular aggregates. The T_c dependences of v_0 and I_n for the nodular aggregates are similar to those of spherulites ordinarily observed by optical microscopy. The T_c dependences of ξ_0 and τ_0 can be also calculated by obtained v_0 and I_n in Fig. 3(b). ξ_0 increases with increasing T_c, but is smaller than the size of spherulites in a micrometer scale. τ_0 decrease with increasing T_c. The T_c dependence of τ_0 shows that the system is dominated by translational diffusion as mentioned above.

The kinetics for the nodular aggregates is similar to those of spherulites as mentioned above, and thus it is very interesting to compare the growth kinetics of nodular aggregates and spherulites. The T_c dependence of v_0 can be directly compared with that of the spherulitic growth rate u. Figure 3(c) shows the T_c dependences of v_0 and u. The secondary

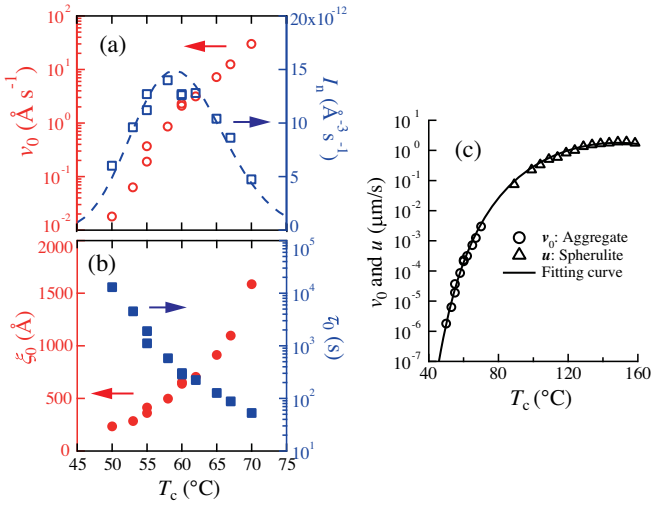

FIG. 3. (a) T_c-dependent v_0 and I_n for the aggregation region of nodules, and (b) T_c-dependent ξ_0 and τ_0 calculated from the values of v_0 and I_n. (c) The comparison of the T_c dependences of v_0 and u. A broken curve in (a) and a solid curve in (c) are fitting curves for I_n and u, respectively.

nucleation type spherulitic growth rate u for polymer is well written as $u = u_0\beta \exp\{-[K_G/(T_c(T_m^0 - T_c))]\}$, where u_0 and K_G are constants, T_m^0 is the equilibrium melting temperature, and β is the Vogel-Fulcher-Tammann type diffusion term, given by $\beta = \exp\{-[U/(R(T_c - T_V))]\}$, U is a constant, R is the ideal gas constant, and T_V is the Vogel temperature. $U = 1500$ cal and $T_V = T_g - 30$ K are used as typical values for polymer materials [12]. When $T_m^0 = 277$°C [47], the fitting growth rate curve in Fig. 3(c) shows that the T_c dependence of v_0 is a natural extrapolation of that of u to the high supercooling region. K_G is estimated as 4.23×10^5 K^2.

The homogeneous nucleation rate is given as $I_n = I_{n0}\beta \exp\{-[K_I/(T_c(T_m^0 - T_c)^2)]\}$, where K_I is a constant. The fitting curve with $K_I = 9.97 \times 10^8$ K^3 well reproduces the T_c dependence of I_n in Fig. 3(a). A general polymer crystallization model often gives the situation in which the chain-folded nucleation and then multinucleation based lamellar growth. The situation gives $K_I = \{[32\zeta_e\zeta_s^2(T_m^0)^2]/[k_B\Delta H^2]\}$ and $K_G = (2b\zeta_e\zeta_s T_m^0/k_B\Delta H)$, where ζ_e and ζ_s are the folding and the lateral surface energies, respectively, k_B is the Boltzmann constant and ΔH is the enthalpy difference between crystal and amorphous, and b is the thickness of the stem added on the substrate [12]. The relation between ζ_s and ΔH is given as the Thomas-Staveley (TS) relation [48,49], $\zeta_s = \alpha_{\mathrm{TS}}(ab)^{0.5}\Delta H$, where α_{TS} is constant depending on material properties and a is the width of the stem. Assuming $a \fallingdotseq b$, the TS relation leads $K_I/K_G = 16\alpha_{\mathrm{TS}}T_m^0$ and gives $\alpha_{\mathrm{TS}} = 0.27$. The value of α_{TS} is estimated as 0.3–0.4 for ordinary organic materials [48] and 0.1–0.3 for polymers [49,50]. Thus the T_c dependence of I_n also can be represented by the parameters estimated for the lamellar growth u.

The results of v_0, u, and I_n show that the nucleation rate and growth rate of the aggregation region composed of the discretely located nodules can be described using the parameter estimated for the ordinary lamellar growth and provide a following possible scenario for polymer crystallization. The precursor forms just before the nucleation of the nodular aggregation region or of the crystalline lamella, and in front of the growth face of the aggregation region or the lamella. The precursor is incorporated and transforms into a part of the crystalline lamella well above T_g, while it transforms into the crystalline nodule without transforming into the lamellae near T_g.

The homogeneous nucleation process near T_g has been detected by fast differential scanning calorimetry (fast-DSC) [34]. Our results strongly suggest that the homogeneous nucleation detected by fast-DSC comes from the formation of the aggregation regions of the nodules.

The lamellae composed of the crystalline nodules (small globules) have been observed by electron microscopy [51–53]. Strobl have proposed the model that the lamellae form with attaching the small globules at the growth front through the mesophase [30]. Miyoshi and coworkers [32,33] have reported using nuclear magnetic resonance (NMR) techniques that there are chain foldings even in the nodules of isotactic polypropylene and that the NMR results are direct evidence of the cooperative coarsening of the nodules. Muthukumar's model explains the early stage of nucleation by precursor "baby nuclei" followed by a cooperative coarsening of these multiple nuclei on the basis of the entropic effect of the polymer chain between baby nuclei by theoretical and simulation methods [24–26].

These results are consistent with our scenario. The reported models [26,30], however, explain the formation of the lamella composed of the nodules connected to each other in the direction parallel to the growth face, but do not discuss the nucleation and growth of the aggregation composed of the "discretely" located nodules. Our results have the potential to develop these models. It is unique in classical crystallization that the nucleation and growth mechanism of the aggregate of the discretely located nodules and that of the spherulite are the same since the general crystallization models are based on the attachment of molecules to the growth front. It is important to investigate the relation between our results and the two-step crystallization process with forming precursors in the other system [1–11].

In summary, in order to clarify the growth kinetics of the crystalline nodular aggregates, the crystallization of PTT from the melt state has been investigated by x-ray techniques and optical microscopy. The analyses of the SAXS results using the KJMA and Sekimoto's theories reveal that the growth kinetics of the aggregation region is

three-dimensional homogeneous nucleation. Furthermore, the growth velocity of the aggregation region follows the same dependence on T_c with spherulites, and the parameters used for the growth rate can also represent the T_c dependence of the nucleation rate of the aggregation region. The results might indicate the evidence of the precursors dominating the formation of crystal domains.

This work was partially supported by JSPS KAKENHI Grant No. JP25800236. The x-ray experiments were performed at the BL-40B2 of SPring-8 with the approval of the Japan Synchrotron Radiation Research Institute (JASRI) (Proposals No. 2017A1497, No. 2018A1083, No. 2018B1377, No. 2018B1454, No. 2019A1301, No. 2019B1318, No. 2020A1111, No. 2020A1113, and No. 2021A1413).

*konishi.takashi.8c@kyoto-u.ac.jp

[1] K. Schätzel and B. J. Ackerson, Phys. Rev. E **48**, 3766 (1993).
[2] P. R. ten Wolde and D. Frenkel, Science **277**, 1975 (1997).
[3] U. Gasser, E. R. Weeks, A. Schofield, P. N. Pusey, and D. A. Weitz, Science **292**, 258 (2001).
[4] H. J. Schöpe, G. Bryant, and W. van Megen, Phys. Rev. Lett. **96**, 175701 (2006).
[5] J. R. Savage and A. D. Dinsmore, Phys. Rev. Lett. **102**, 198302 (2009).
[6] A. Sanz, A. Nogales, I. Puente-Orench, M. Jimenez-Ruiz, and T. A. Ezquerra, Phys. Rev. Lett. **107**, 025502 (2011).
[7] T. Schilling, H. J. Schöpe, M. Oettel, G. Opletal, and I. Snook, Phys. Rev. Lett. **105**, 025701 (2010).
[8] J. Russo and H. Tanaka, Sci. Rep. **2**, 505 (2012).
[9] T. Kawasaki and H. Tanaka, Proc. Natl. Acad. Sci. U.S.A. **107**, 14036 (2010).
[10] J. F. Lutsko and G. Nicolis, Phys. Rev. Lett. **96**, 046102 (2006).
[11] J. F. Lutsko, J. Chem. Phys. **136**, 034509 (2012).
[12] J. D. Hoffman, G. T. Davis, and J. I. Lauritzen, in *Treatise on Solid State Chemistry*, edited by N. B. Hannay (Plenum, New York, 1976), Vol. 3, p. 497.
[13] G. Allegra, J. Chem. Phys. **66**, 5453 (1977).
[14] K. Fukao and Y. Miyamoto, Phys. Rev. Lett. **79**, 4613 (1997).
[15] M. Soccio, A. Nogales, N. Lotti, A. Munari, and T. A. Ezquerra, Phys. Rev. Lett. **98**, 037801 (2007).
[16] M. Imai, K. Mori, T. Mizukami, K. Kaji, and T. Kanaya, Polymer **33**, 4451 (1992).
[17] N. J. Terrill, P. A. Fairclough, E. Towns-Andrews, B. U. Koanschek, R. J. Young, and A. J. Ryan, Polymer **39**, 2381 (1998).
[18] K. Kaji, K. Nishida, T. Kanaya, G. Matsuba, T. Konishi, and M. Imai, Adv. Polym. Sci. **191**, 187 (2005).
[19] T. A. Ezquerra, E. López-Cabarcos, B. S. Hsiao, and F. J. Baltà-Calleja, Phys. Rev. E **54**, 989 (1996).
[20] Y. Akpalu, L. Kielhorn, B. S. Hsiao, R. S. Stein, T. P. Russell, J. van Egmond, and M. Muthukumar, Macromolecules **32**, 765 (1999).
[21] S. Sasaki, K. Tashiro, M. Kobayashi, Y. Izumi, and K. Kobayashi, Polymer **40**, 7125 (1999).
[22] P. D. Olmsted, W. C. K. Poon, T. C. B. McLeish, N. J. Terrill, and A. J. Ryan, Phys. Rev. Lett. **81**, 373 (1998).
[23] Z. G. Wang, B. S. Hsiao, E. B. Sirota, P. Agarwal, and S. Srinivas, Macromolecules **33**, 978 (2000).
[24] C. Liu and M. Muthukumar, J. Chem. Phys. **109**, 2536 (1998).
[25] P. Welch and M. Muthukumar, Phys. Rev. Lett. **87**, 218302 (2001).
[26] M. Muthukumar, Phil. Trans. R. Soc. A **361**, 539 (2003).
[27] P. M. Welch, J. Chem. Phys. **146**, 044901 (2017).
[28] R. H. Gee, N. M. Lacevic, and L. E. Fried, Nat. Mater. **5**, 39 (2006).
[29] P. Panine, E. Di Cola, M. Sztucki, and T. Narayanan, Polymer **49**, 676 (2008).
[30] G. Strobl, Rev. Mod. Phys. **81**, 1287 (2009).
[31] C. Luo and J. U. Sommer, Macromolecules **44**, 1523 (2011).
[32] Y. L. Hong, S. Yuan, Z. Li, Y. Ke, K. Nozaki, and T. Miyoshi, Phys. Rev. Lett. **115**, 168301 (2015).
[33] S. Yuan, Z. Li, Y Hong, Y. Ke, J. Kang, A. Kamimura, A. Otsubo, and T. Miyoshi, ACS Macro Lett. **4**, 1382 (2015).
[34] C. Schick, R. Androsch, and J. W. P. Schmelzer, J. Phys. Condens. Matter. **29**, 453002 (2017).
[35] W. T. Chuang, W. B. Su, U. S. Jeng, P. D. Hong, C. J. Su, C. H. Su, Y. C. Huang, K. F. Laio, and A. C. Su, Macromolecules **44**, 1140 (2011).
[36] J. B. Jheng, W. T. Chuang, P. D. Hong, Y. C. Huang, U. S. Jeng, C. J. Su, and G. R. Pan, Polymer **54**, 6242 (2013).
[37] T. Konishi, D. Okamoto, D. Tadokoro, Y. Kawahara, K. Fukao, and Y. Miyamoto, Phys. Rev. Mater. **2**, 105602 (2018).
[38] A. N. Kolmogorov, Izv. Akad. Nauk. SSSR Ser. Mat. **3**, 355 (1937).
[39] W. A. Johnson and R. F. Mehl, Trans. Metall. Soc. AIME **135**, 416 (1939).
[40] M. Avrami, J. Chem. Phys. **7**, 1103 (1939).
[41] M. Avrami, J. Chem. Phys. **8**, 212 (1940).
[42] M. Avrami, J. Chem. Phys. **9**, 177 (1941).
[43] See Supplemental Material at http://link.aps.org/supplemental/10.1103/PhysRevLett.128.107801 for the WAXD results of PTT isothermally crystallized at 60°C from the melt state, a procedure for obtaining the volume fractions of the aggregation region and the crystalline nodules from the SAXS result, the structure factor for the aggregation regions of the growth rate v_0 with the Gaussian distribution, and the SAXS results of PTT for several T_c, which includes Ref. [44].
[44] S. Poulin-Dandurand, S. Pérez, J. Revol, and F. Brisse, Polymer **20**, 419 (1979).
[45] J. K. Percus and G. J. Yevick, Phys. Rev. **110**, 1 (1958).
[46] K. Sekimito, Physica (Amsterdam) **135A**, 328 (1986).
[47] P. Srimoaon, N. Dangseeyun, and P. Supaphol, Eur. Polym. J. **40**, 599 (2004).

[48] D. G. Thomas and L. A. K. Staveley, J. Chem. Soc. **889**, 4569 (1952).
[49] J. D. Hoffman, R. L. Miller, H. Marand, and D. B. Roitman, Macromolecules **25**, 2221 (1992).
[50] T. Konishi, W. Sakatsuji, and Y. Miyamoto, Polymer **119**, 160 (2017).
[51] T. Hugel, G. Strobl, and R. Thomann, Acta Polym. **50**, 214 (1999).
[52] Y. Wang, B. Chen, K. E. Evans, and O. Ghita, Mater. Lett. **184**, 112 (2016).
[53] Y. Wang, B. Chen, K. E. Evans, and O. Ghita, Sci. Rep. **8**, 1314 (2018).

Correction: The values of v_0 and $\bar{v}_0$ in the caption to Fig. 1, in the third and eighth sentences after Eq. (4), and in related material inside the Supplemental Material contained errors and have been set right.